Progress In Electromagnetics Research, Vol. 110, 353–369, 2010

DETECTION AND IMAGING OF HUMAN BEINGS BEHIND A WALL USING THE DORT METHOD

M. Davy, T. Lepetit, J. de Rosny, C. Prada, and M. Fink

Institut Langevin, ESPCI ParisTech, CNRS UMR 7587
Laboratoire Ondes et Acoustique
Université Denis Diderot Paris 7, ESPCI
10 Rue Vauquelin, 75231 Paris Cedex 05, France

Abstract—In recent years, through the wall imaging has become a topic of intense research due to its promising applications in police, fire and rescue or emergency relief operations. In this paper, we propose to use the DORT method (French acronym for Decomposition of the Time Reversal Operator) to detect and localize a moving target behind a wall. One of the DORT method major strengths is that detection remains possible through a distorting medium. In this paper, the DORT method is successfully applied to detect and track moving human beings behind a thick concrete wall. The smallest detectable displacement is also investigated.

1. INTRODUCTION

Ultra-Wideband (UWB) through the wall imaging has recently become a topic of intense research as it concerns detection and localization of people behind impenetrable walls. Issues range from rescue operations in rubble to terrorists movements tracking inside a building. An overview of those different aspects can be found in [1, 2]. In those papers, the historical context of the research is outlined, the different stakes of the field are described and some future directions are provided. In this paper, we specifically address the detection and localization of a target moving behind a wall.

Several works dealing with the detection of moving targets in a cluttered environment have already been published [3–5]. In these works, classical array processing methods are applied: beamforming,

Received 17 September 2010, Accepted 1 November 2010, Scheduled 25 November 2010
Corresponding author: Matthieu Davy (matthieu.davy@espci.fr).

back-propagation or time of flight. Here, we propose to use the DORT method. This method was introduced by Prada and Fink in 1994 [6] and is derived from time reversal mirror experiments. It consists in computing the invariants of the Time Reversal Operator (TRO). The method was first developed for ultrasonic applications with arrays of piezo-electric transceivers [6–8]. It has shown its efficiency in several domains like non-destructive evaluation [8], detection in shallow water [9] and medical imaging [10]. The DORT method can be applied to all types of linear waves and has been employed in electromagnetism since 2001 [11–13]. One of the DORT method major strengths is that detection remains possible through distorting media. This property is particularly interesting for through the wall detection.

Time reversal methods have already been applied to through the wall imaging, either numerically [14] or experimentally [4]. In this paper, the DORT method is combined with the MUSIC algorithm to find out scatterers location. Cheney was the first to investigate the use of the MUSIC algorithm for imaging [15] while Lev-Avri and Devaney were the first to combine it with time reversal methods [16]. In addition, some recent papers have underlined the added value of using the MUSIC algorithm for indoor imaging as well as through the wall applications [17, 18]. In this paper, we take advantage of the DORT-MUSIC method's ability to resolve two close scatterers that are less than half a wavelength apart [19]. As a result, with the DORT-MUSIC method, we are able to detect smaller movements than with classical beamforming methods.

This paper is organized as follows. The principles of the DORT method are recalled and the need of a differential measurement is discussed in Section 2. In Section 3, the experimental setup and wall parameters estimation are presented. In Section 4, detection of a human being is demonstrated. Two distinct imaging schemes, incoherent and coherent, are considered and compared. In Section 5, the subwavelength resolution capacity of the DORT-MUSIC method is also tested in the case of two close scatterers. The last part addresses target tracking. This is followed by a conclusion and prospects.

2. INVARIANTS OF THE TIME REVERSAL OPERATOR

We consider two antenna arrays. An array Tx of N^{Tx} antennas is used in emission and an array Rx of N^{Rx} antennas is used in reception. Let k_{lm} be the recorded signal after propagation between antenna $\#l$ of the Tx array and antenna $\#m$ of the Rx array. All those signals are used to build the $N^{Tx} \times N^{Rx}$ inter-elements-response matrix or

transfer matrix, denoted $\mathbf{K}$. For example, when a vector $\mathbf{E}$ is emitted, the received vector $\mathbf{R}$ is given by $\mathbf{R} = \mathbf{KE}$. The so-called Time Reversal Operator (TRO) is defined as $\mathbf{K^H K}$ (superscript $^{\mathbf{H}}$ stands for conjugate-transpose). The TRO is Hermitian and consequently diagonalizable. The eigenvectors of the TRO can be interpreted as invariants of the time reversal process [6].

The singular value decomposition (SVD) of the transfer matrix $\mathbf{K}$ can be used to compute the eigenvectors of the TRO $\mathbf{K^H K}$. It is written:

$$\mathbf{K} = \sum_{j=1}^{\min\left(N^{Tx},N^{Rx}\right)} \left(\mathbf{u}_j^{Rx}\right) \sigma_j \left(\mathbf{u}_j^{Tx}\right)^H \tag{1}$$

Indeed, the singular vectors $\mathbf{u}_j^{Tx}$ are the eigenvectors of the Time Reversal Operator $\mathbf{K^H K}$ while the singular values σ_j are the square roots of its eigenvalues. Besides, if the roles of the arrays are switched, i.e., Rx array is used in emission and Tx array in reception, the Time Reversal Operator becomes $\mathbf{KK^H}$. It can then be shown that the singular vectors $\mathbf{u}_j^{Rx}$ are the eigenvectors of this second TRO. In practice, the SVD is used to localize the scatterers as explained in part 4.

In our experiments, load-bearing walls are considered. Those walls are too thick and reflective to allow the extraction of the target response directly from the backscattered signal. Indeed, the target response is totally embedded in the tail of the wall reflection. Removal of the wall echoes is therefore needed. To that end, the transfer matrix $\mathbf{K}$ is recorded at two different times τ and $\tau\delta\tau$, and the two transfer matrices are subtracted:

$$\delta\mathbf{K}(\tau + \delta\tau) = \mathbf{K}(\tau + \delta\tau) - \mathbf{K}(\tau) \tag{2}$$

Assuming that the wall echoes are time invariant, they are cancelled in the difference matrix and only the signal reflected from the moving target remains. However, there is an exception to echo cancelation for stationary furniture which lies in the shadow of the target. Yet, these echoes always come after the ballistic target echo and can thus be removed via time windowing. Besides, in the case of small scatterers, the rank of $\mathbf{K}$ is equal to the number of scatterers. Due to the substraction, $\delta\mathbf{K}$ can be seen as the response of two scatterers at two different positions. Therefore, the rank of $\delta\mathbf{K}$, or in other words the number of significant singular values, equals 2.

3. EXPERIMENTAL CONFIGURATION

3.1. Experimental Setup

We use a Multiple-Input Multiple-Output (MIMO) experimental setup consisting of two arrays each composed of 7 Vivaldi antennas. Contrary to previous setups [20], the Tx and Rx arrays are not side by side but interlaced (see Figure 1). The distance between two consecutive Vivaldi antennas is 6 cm. The antennas are efficient between 1.5 and 8 GHz and are vertically polarized. The antenna arrays are connected to a vector network analyzer through two electro-mechanical switches in order to measure the $S_{12}(\omega)$ parameter between each Tx antenna and each Rx antenna. Time-domain signals $S_{12}(t)$ are obtained *via* Fast Fourier Transform (FFT). The analyzer delivers a power of +12 dBm. In addition, the antennas are set parallel to the wall at a distance of 6 cm. They are close to the wall to make sure enough power is transmitted through the wall. However, they are not positioned *against* the wall in order to mimick operational conditions.

3.2. Wall Parameters

Independently of the array processing method (arrival times, beamforming, back-propagation, etc.), wall parameters have to be accurately estimated to localize the target. Indeed, an error in their estimation induces a shift on target location [21, 22]. Therefore, a key point is the experimental estimation of wall parameters: permittivity ε_r and thickness d. The effect of the wall becomes more important

Figure 1. Experimental setup consisting of two arrays of 7 Vivaldi antennas connected to a vector network analyzer by two electromechanical switches. The blue foam is absorbing material to decrease parasitic echoes.

as the wall's electrical thickness $d\sqrt{\varepsilon_r}$ increases. Indeed, the travel times are then very different from free space propagation. Many papers propose methods to estimate these wall parameters. Obviously, methods based on the analysis of waves transmitted through the wall cannot be used in operational devices. Other methods rely on the signal reflected from the target [23–25], but are therefore dependent on its presence. In this article, we propose to deduce the parameters using a time of flight method. We take advantage of the echoes backscattered from the front and back interfaces of the wall. A simple ray model and a non-linear minimization algorithm are designed to extract the thickness and permittivity. This method assumes sufficiently broadband antennas such that the echoes from the front and back interfaces are temporally separated. The roundtrip propagation time in the wall ($2d\sqrt{\varepsilon_r}/c$) must therefore be larger than the pulse length (i.e., the inverse of the bandwidth). As shown in [23], arrival times method are very sensitive to the wall electrical thickness $d\sqrt{\varepsilon_r}$, but not to d and ε_r individually. However, this assumption is not a major problem, in our case, as object localization is primarily influenced by the wall electrical thickness when angles of incidence are smaller than 20° [23].

On Figure 2, the envelope of the experimental response between two antennas is plotted versus time. Four peaks appear distinctly between 0 and 10 ns. The first one at 3 ns, whose amplitude is low because the Tx and Rx antennas are far apart, is associated to the direct path between the antennas. The second one at 3.4 ns corresponds to the reflection off the front interface. The third one at 4.95 ns is probably due to a strong heterogeneity inside the wall (air hole, metallic structure ...). The last one at 6.7 ns comes from the

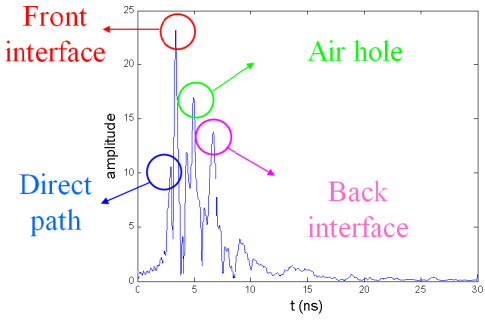

Figure 2. Envelope of the response between antenna #5 of the Tx array and #1 of the Rx array B versus time.

back interface. Travel time measurements on other antennas prove that the third and fourth peaks cannot be due to multiple reflections inside the wall.

The front interface arrival times are first used to estimate the distance between each antenna array and the wall. The back interface arrival times are then used to find out the effective permittivity and thickness of the wall.

The first step of our model consists in expressing the distances travelled in the air and in the wall using a simple ray model. On Figure 3, we observe that these distances do not depend on the position of the wall between A and P.

The approximation given in [26] is used to work out the theoretical distances. With the notation displayed on Figure 3, the optical path length AB_3 and B_3P are given by:

$$\begin{aligned} AB_3 &= \sqrt{\left(1-\sqrt{\frac{1}{\varepsilon_r}}\frac{d}{y}\right)^2 (x-x_1)^2 + (y-d)^2} \\ \text{and } B_3P &= d\sqrt{1+\frac{1}{\varepsilon_r}\frac{(x-x_1)^2}{y^2}} \end{aligned} \tag{3}$$

The arrival times are then obtained from those expressions and the travel time inside a Vivaldi antenna. This last has been experimentally measured as 0.85 ns. Wall parameters are then worked out by the minimization of a cost function. The sum of squares of the differences between the theoretical and experimental arrival times is used. It

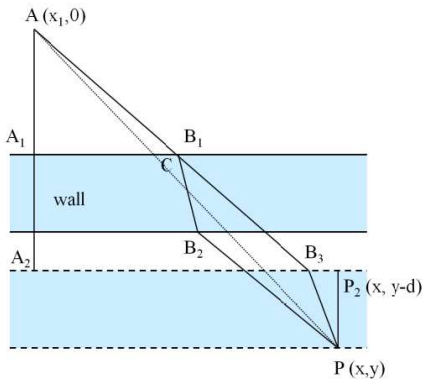

Figure 3. Ray paths used in the computation of the coordinates of the inflection point for two interfaces.

depends on ε_r and d and is written:

$$W(d, \varepsilon_r) = \sum_{i=1}^{N1} \sum_{j=1}^{N2} \left[(\tau_{\exp})_{i,j} - (\tau_{\text{th}}(d, \varepsilon_r))_{i,j} \right]^2 \quad (4)$$

In Equation (4), $\tau_{\exp}$ stands for the experimental estimation and $\tau_{\text{th}}(d, \varepsilon_r)$ for the theoretical estimation of the back interface arrival times.

On Figure 4, the inverse of the cost function $W(d, \varepsilon_r)$ is displayed. The maximum is reached for a thickness $d = 36$ cm and a permittivity $\varepsilon_r = 2.36$. Those values can be compared to the actual thickness of 27.5 cm and permittivity, measured in transmission through the wall, of 4.22. As stated above, the arrival time method is not adapted to measure d and ε_r individually. Nevertheless it accurately estimates the electrical thickness of the wall $d\sqrt{\varepsilon_r}$. This property clearly appears on Figure 4 where the cost function is maximum when the product $d\sqrt{\varepsilon_r}$ is constant and equal to 0.55. This value is close to 0.57, the electrical thickness found in transmission. As $d\sqrt{\varepsilon_r}$ is the relevant parameter for imaging, its estimation is a key point for target localization.

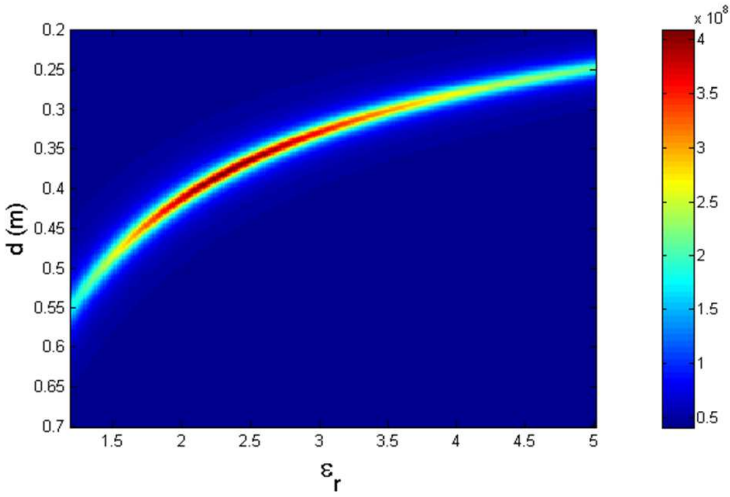

Figure 4. Inverse of the cost function $W(d, \varepsilon_r)$ with respect to the permittivity ε_r and thickness d of the wall. It is maximum for a wall electrical thickness $d\sqrt{\varepsilon_r}$ of 0.55.

4. BEHIND THE WALL TARGET IMAGING

4.1. Detection of a Human Being

In the following experiment, the target is a human being. Antenna arrays have also been set closer to the wall compared to Section 3.2. Due to attenuation inside the wall, the highest frequencies (from 4 to 8 GHz) do not contribute to the measured signals. Hence, only the frequencies below 4 GHz are taken into account. On Figure 5, the signal obtained after subtraction is displayed. Thanks to the subtraction, the wavefront reflected off the target clearly appears at 6.8 ns. Note that, in this experiment, the first transfer matrix $\mathbf{K}(\tau)$ is measured when the target is not in the field of view.

A sliding time window can be applied on the signals $S_{12}(t)$. The width ΔT of the square window is chosen equal to 1 ns. After FFT of the windowed signals, the inter-elements response matrices $\delta\mathbf{K}(f,T)$ are obtained. Time T is the centre position of the time window. The singular values $\sigma_n(f,T)$ are computed from matrices $\delta\mathbf{K}(f,T)$. On Figure 6, they are plotted at 2.2 GHz. Two peaks significantly emerge from the noise. The first one corresponds to the front interface echoes remaining after subtraction, due to a lack of dynamic range, while the second one corresponds to the target echoes (at 6.8 ns). The time-reversal invariants (i.e., the singular vectors) associated to this second peak are, in the following, naturally used to compute the position of the target.

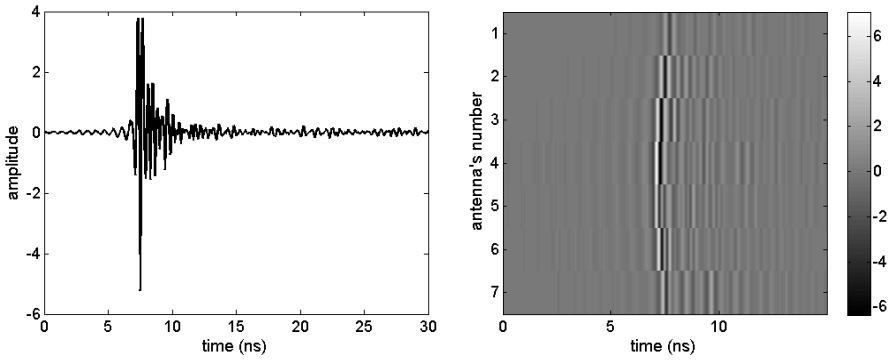

(a) (b)

Figure 5. (a) Signal between antenna #3 of the transmit array and antenna #4 of the receive array, after subtraction between two matrices $\mathbf{K}$ acquired with and without a human being behing the concrete wall. (b) Gray level representation of the signal from antenna #4 of the transmit array on the 7 antennas of the receive array.

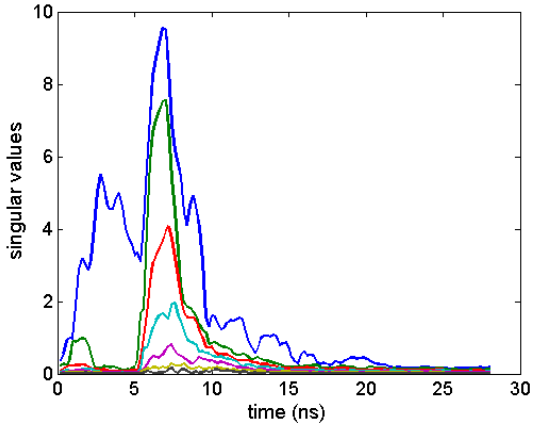

Figure 6. Singular values $\sigma_n(f,T)$ with respect to the temporal window start time T.

One or several singular values can be associated to a scatterer depending on its size. Several papers have been published in which singular values are computed as a function of scatterer's size and location relative to that of the transmitting and receiving antennas [20, 27–29]. The main conclusion is that for a given polarization, there are as many singular values as focal spots on the target. In the classical Rayleigh limit, the focal spot width equals $\lambda f/D$, where D is the array aperture and f the focal length [10]. In our experiment, the transverse size of the body, i.e., the scatterer, is about 48 cm. As a result, several singular values emerge from the noise on Figure 6. Most of the time, the first singular vectors, both the Tx one and Rx one, are mainly due to monopolar scattering. Consequently, the back-propagation of these time-reversal invariants gives rise to a monopolar focus located at the target position [20].

4.2. Incoherent Back-propagation of the Singular Vectors

In order to localize the target(s), the singular vectors are numerically back-propagated into the medium. To that end, the experimental singular vectors are correlated with the vectors deduced from the Green's function. The correlation function at location $\mathbf{r}$ is given by:

$$\mathbf{W}_1(\mathbf{r}) = \left|\left\langle \mathbf{u}_n^{Tx} * \left|\tilde{\mathbf{G}}^{Tx}(\mathbf{r})\right\rangle\right|^2 + \left|\left\langle \mathbf{u}_n^{Rx}\left|\tilde{\mathbf{G}}^{Rx}(\mathbf{r})\right\rangle\right|^2 \quad (5)$$

where $\tilde{\mathbf{G}}^{Tx}(\mathbf{r})$ (respectively $\tilde{\mathbf{G}}^{Rx}(\mathbf{r})$) stands for the normalized vector of the phases of the Green functions from the antennas of the Tx

(resp. Rx) array to the point to be imaged. The singular vectors $\mathbf{u}_n^{Tx}$ (respectively $\mathbf{u}_n^{Rx}$) are associated to the transmit (resp. receive) array. The notation $\langle \mathbf{A}|\mathbf{B}\rangle$ is the Hermitian scalar product, i.e., $\mathbf{A}^H\mathbf{B}$. Therefore, an estimation of the Green's function that describes the propagation from the antennas to a point behind the wall is required. To be accurate, for the correlations only the phases of the Green functions are considered, their amplitudes being set to 1. Indeed, the $1/\sqrt{r}$ decay of those functions is not useful for target location. Considering the wall as homogeneous, from Equation (3), the Green's function between an antenna at position $A(X_i,0)$ and a point $P(x,y)$ behind the wall is given by:

$$\tilde{G}(x,y) = \exp\left(ik_0 AB_3\right)\exp\left(i\sqrt{\varepsilon_r}k_0 B_3 P\right) \tag{6}$$

Hence, wall parameters ε_r and d, worked out in paragraph 3, are essential to an accurate estimation of the Green functions' phase.

Some important secondary lobes may appear on the image due to the incoherent sum of the contributions coming from Tx and Rx arrays. In the next paragraph, a way to reduce those lobes is presented.

4.3. Coherent Back Propagation of the Singular Vectors

To reduce side lobes level, one wants to add coherently the Tx and Rx contributions, i.e., $\left\langle \mathbf{u}_n^{Tx}* \middle|\, \tilde{\mathbf{G}}^{Tx}(\mathbf{r})\right\rangle + \left\langle \mathbf{u}_n^{Rx} \middle|\, \tilde{\mathbf{G}}^{Rx}(\mathbf{r})\right\rangle$. However, there exists an arbitrary phase between the singular vectors $\mathbf{u}_n^{Tx}$ and $\mathbf{u}_n^{Rx}$. As a result, the contributions of the two arrays in Equation (8) may not be in phase at the focus. In order to ensure constructive interferences at the focal point, a phase shift $\delta\Phi$ is added to $\mathbf{u}_n^{Tx}$. It is determined by minimizing the distance between the unwrapped phase laws of the two singular vectors. As the Rx and Tx singular vectors are concatenated, their respective phases must be continuous on the whole array as shown on Figure 7.

The image resulting from the back-propagation of the two *in phase* singular vectors is then given by:

$$W_2(\mathbf{r}) = \left|\left\langle \mathbf{u}_n^{Tx}* \middle| \tilde{\mathbf{G}}^{Tx}(\mathbf{r})\right\rangle + e^{\mathrm{i}\delta\phi}\left\langle \mathbf{u}_n^{Rx} \middle| \tilde{\mathbf{G}}^{Rx}(\mathbf{r})\right\rangle\right|^2 \tag{7}$$

The two contributions are now in phase at the focus. Thanks to the coherent summation, the secondary lobes are now much smaller (see Figure 8).

This lobe reduction is useful in the case of several targets because it reduces the risk of false alarm, i.e., when a side lobe is confused with a target. In the following, only the coherent back-propagation will naturally be used.

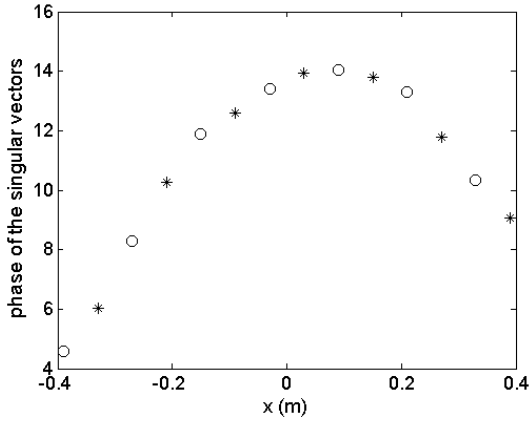

Figure 7. Phase of $\mathbf{u}_n^{Tx}(o)$ and $\mathbf{u}_n^{Rx}(*)$ on the whole array at 2.6 GHz. The arbitrary phase between $\mathbf{u}_n^{Tx}$ and $\mathbf{u}_n^{Rx}$ has been chosen in order to obtain a continuous phase.

5. MUSIC ESTIMATOR AND SUBWAVELENGTH RESOLUTION

In this paragraph, the spatial resolution that can be achieved with the DORT-MUSIC method is investigated [19]. By spatial resolution, we mean the minimum distance between two scatterers that can be separated. In this experiment, the targets consist of aluminum cylinders. Due to their small diameter (5 cm), only one singular value is significant when $\delta\mathbf{K}$ is the difference between matrices $\mathbf{K}$ measured with and without one cylinder behind the wall. With two cylinders, the rank of $\delta\mathbf{K}$ equals 2. However, the closer the targets are, the smaller the second singular value is. When the targets are closer than the Rayleigh criterion, W_2 shows only one spot instead of two. One may therefore think there is only one target. To increase the resolution beyond the Rayleigh limit, we use the DORT-MUSIC method.

In the DORT-MUSIC method, the singular vectors are partitioned into signal and noise singular vectors, which form two orthogonal subspaces. The signal subspace, as opposed to the noise subspace, consists of the singular vectors associated to the targets. The dimension p of the signal subspace is given by the number of non-zero singular values. As such, here p equals two. Note that an accurate estimation of the signal subspace dimension is critical to achieve a good spatial resolution with the DORT-MUSIC method. Used with coherent singular vectors, i.e., after the estimation of $\delta\phi$, the MUSIC

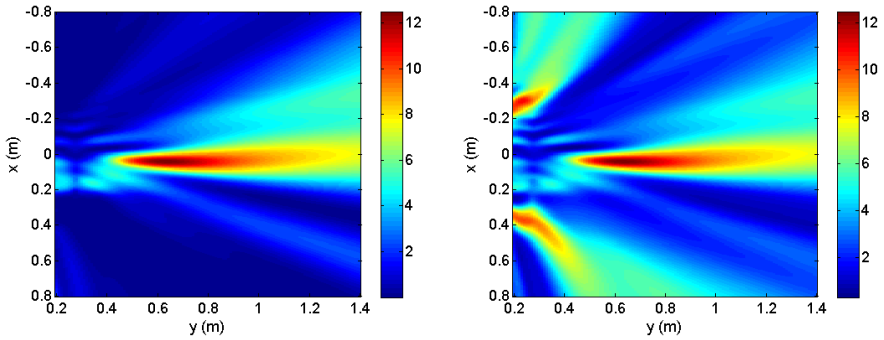

Figure 8. (a) coherent back-propagation of the first singular vector (W_2); (b) likewise but for an incoherent back-propagation (W_1); note that colorscales are the same.

estimator is written:

$$W_{MU}(r) = \frac{1}{\sum_{n=3}^{7} \left| \left\langle \mathbf{u}_n^{Rx} * \;\middle|\; \tilde{\mathbf{G}}^{Rx}(\mathbf{r}) \right\rangle + e^{\mathrm{i}\delta\phi} \left\langle \mathbf{u}_n^{Tx} \;\middle|\; \tilde{\mathbf{G}}^{Tx}(\mathbf{r}) \right\rangle \right|^2} \tag{8}$$

Due to the signal and noise subspace orthogonality, when $\mathbf{r}$ corresponds to the position of a scatterer, all scalar products between noise singular vectors and Green functions vectors are null. Theoretically, the MUSIC estimator $W_{MU}(r)$ diverges at each scatterer's position. However, due to noise and model mismatches, $W_{MU}(r)$ is strongly peaked but not infinite. The DORT-MUSIC method identifies all scatterers at once. On Figure 9(a), the MUSIC estimation is plotted versus the x and y-axis at 1.95 GHz, i.e., $\lambda = 15.4$ cm. The targets were placed right next to each other: their centres are separated by only 5.1 cm, i.e., $\lambda/3$. Two peaks appear on Figure 9(a), corresponding to their positions. As expected, a distance between the two peaks of 5.1 cm is found. Note that a criterion to estimate the noise level above which the subwavelength spatial resolution fails has previously been given [30]. To compare with, the same data have been processed with a beamforming algorithm (Figure 9(b)). In this case, only one bright spot clearly appears.

6. BEHIND THE WALL TARGET TRACKING

In this paragraph, we track the movements behind a wall of one of the above-described aluminum cylinders. Ten $\mathbf{K}_i$ matrices are acquired

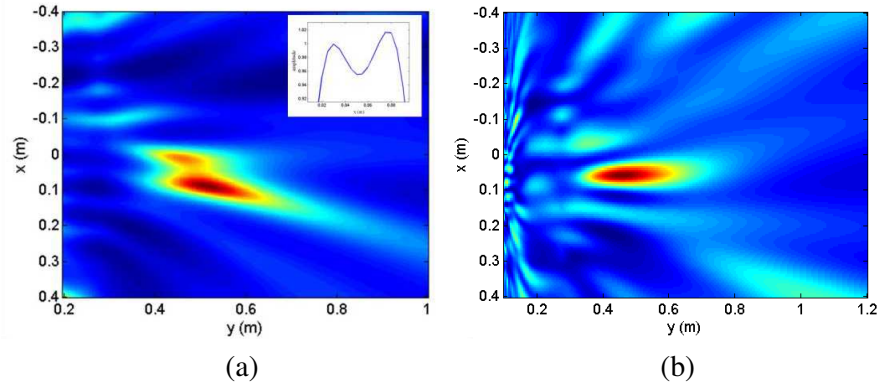

Figure 9. (a) Coherent MUSIC back-propagation in the case of 2 cylinders (diameter 5 cm) spaced by 5.1 cm at 1.95 GHz ($\lambda = 15.4$ cm). The insert (top-right) is a cut along the x-axis at $y = 45$ cm. (b) Coherent beam-forming method.

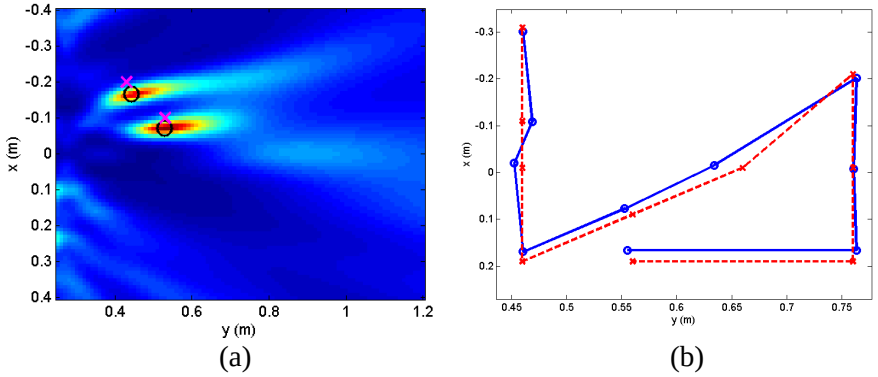

Figure 10. (a) Image associated to the target movement #4. (b) Reconstructed track of the target behind the wall. The dotted line with x markers stands for the theoretical locations and the bold line with o markers for the reconstructed locations.

for ten different positions $\mathbf{r}_i$ of the cylinders. The differential operator is obtained by subtracting the ith matrix to the $(i-1)$th matrix: $\delta\mathbf{K}_i = \mathbf{K}_i - \mathbf{K}_{i-1}$. For each $\delta\mathbf{K}_i$, two distinct non-zero singular values appear which are associated to the two locations $\mathbf{r}_i$ and $\mathbf{r}_{i-1}$ of the target. The MUSIC algorithm, by considering two singular values as belonging to the signal subspace, creates two spots associated to each

target's location, as shown on Figure 10(a). This process leads to an accurate step by step reconstruction of the target motion, as illustrated on Figure 10(b). The smallest detectable movement is directly linked to the spatial resolution that can be achieved with the DORT-MUSIC method. The main added value of this method is then to image subwavelength target displacements.

For an extended moving scatterer we can use, theoretically, the first two monopolar singular vectors just like for the aluminum cylinder. The other multipolar singular values can be included in the noise subspace in order to track the human being using the MUSIC estimator.

7. DISCUSSION

In this paper, we have used the DORT-MUSIC method for through the wall imaging. This method has several advantages compared to classical time reversal [4]. First, the use of several antennas both in emission and reception yields a higher Signal to Noise Ratio (SNR) through the singular value decomposition of the transfer matrix. Indeed, the SVD permits the decomposition into orthogonal signal and noise subspaces. It has been shown that the SNR increases as the square-root of the number of antennas for a given power emitted by the Tx array [9]. Furthermore, the use of the MUSIC estimator, unlike classical time reversal, allows the resolution of two close scatterers. Close here means separated by a subwavelength distance.

As seen on Figure 9, the major strength of the DORT-MUSIC is to find out the position of sub-resolved scatterer in comparison with linear array signal processing (such as beam-forming). However, measuring the full transfer matrix is more time consuming than beam-forming. Furthermore, MUSIC is much more sensitive to noise and mismatch.

In our setup, target tracking is not done in real-time. Indeed, the measurement time is limited by the switching time of the electromechanical switches (50 ms), the number of transmit and receive antennas and the number of measured frequencies. The commutation time of the switches can be dramatically reduced with solid-state switches (< 100 ns). Nevertheless, scanning in depth beyond a wall requires a long acquisition time. This results in a small frequency step for the network analyzer. This frequency step δf is linked to the total time of flight ΔT by $\delta f = 1/\Delta T$. While a larger frequency step would reduce the measurement time, it would also limit the scanning range of our radar.

However, the main limitation is due to the total sweep time. Indeed, each frequency point in itself needs a large enough sweep time

in order to obtain a decent SNR. In our case, it equals 20 µs. Reducing this time is not possible because it would result in a lower SNR and therefore a lower dynamic range, which is just enough to ensure a correct cancellation of the front wall reflections. A quantitative study of the effect of the dynamic on the wall echo cancellation is beyond the scope of this paper. Other means of improving the dynamic range (averaging, tighter IF Bandwidth) also increase the measurement time.

8. CONCLUSION

In this article, we have experimentally illustrated the possibility to use a MIMO configuration and UWB signals in order to detect scatterers behind a wall. A time-reversal based method, the DORT method, has been used to detect metallic cylinders as well as human beings behind a concrete wall. Moreover, we have shown under realistic conditions that not only detection but also tracking of a target is feasible. We have also combined the DORT method with the signal processing algorithm MUSIC to improve spatial resolution. This algorithm has been used to image two scatterers separated by a subwavelength distance. It holds the promise of imaging subwavelength displacements. Further work will be aimed at imaging human beings standing still behind a wall.

REFERENCES

1. Baranoski, E. J., "Through-wall imaging: Historical perspective and future directions," *Journal of the Franklin Institute*, Vol. 345, 556–569, 2008.
2. Griffiths, H. and C. Baker, "Radar imaging for combatting terrorism," *Imaging for Detection and Identification*, 29–48, 2007.
3. Sachs, J., et al., "Detection and tracking of moving or trapped people hidden by obstacles using ultra-wideband pseudo-noise radar," *European Radar Conference 2008, EuRAD 2008*, 408–411, 2008.
4. Maaref, N., P. Millot, X. Ferriéres, C. Pichot, and O. Picon, "Electromagnetic imaging method based on time reversal processing applied to through-the-wall target localization," *Progress In Electromagnetics Research M*, Vol. 1, 59–67, 2008.
5. Soldovieri, R., R. Solimene, and R. Pierri, "A simple strategy to detect changes in through the wall imaging," *Progress In Electromagnetics Research M*, Vol. 7, 1–13, 2009.
6. Prada, C. and M. Fink, "Eigenmodes of the time reversal operator:

A solution to selective focusing in multiple-target media," *Wave Motion*, Vol. 20, 151–163, 1994.

7. Prada, C., et al., "Flaw detection in solid with the D.O.R.T. method," *Ultrasonics Symposium*, Vol. 1, 679–683, 1997.
8. Kerbrat, E., et al., "Detection of cracks in a thin air-filled hollow cylinder by application of the DORT method to elastic components of the echo," *Ultrasonics*, Vol. 40, 715–720, 2002.
9. Prada, C., et al., "Experimental detection and focusing in shallow water by decomposition of the time reversal operator," *The Journal of the Acoustical Society of America*, Vol. 122, 761–768, 2007.
10. Robert, J.-L., et al., "Time reversal operator decomposition with focused transmission and robustness to speckle noise: Application to microcalcification detection," *The Journal of the Acoustical Society of America*, Vol. 119, 3848–3859, 2006.
11. Tortel, H., G. Micolau, and M. Saillard, "Decomposition of the time reversal operator for electromagnetic scattering," *Journal of Electromagnetic Waves and Applications*, Vol. 13, No. 5, 687–719, 1999.
12. Micolau, G. and M. Saillard, "D.O.R.T. method as applied to electromagnetic subsurface sensing," *Radio Sci.*, Vol. 38, 2003.
13. Dubois, A., et al., "Localization and characterization of two-dimensional targets buried in a cluttered environment," S63, 2004.
14. Zheng, W., Z. Zhao, and Z.-P. Nie, "Application of TRM in the UWB through wall radar," *Progress In Electromagnetics Research*, Vol. 87, 279–296, 2008.
15. Cheney, M., "The linear sampling method and the MUSIC algorithm," *Inverse Problems*, Vol. 17, 591–595, 2001.
16. Lev-Ari, H. and A. J. Devaney, "The time-reversal technique re-interpreted: Subspace-based signal processing for multi-static target location," *Proceedings of the 2000 IEEE Sensor Array and Multichannel Signal Processing Workshop*, 509–513, 2000.
17. Yoon, Y.-S. and M. G. Amin, "High-resolution through-the-wall radar imaging using beamspace MUSIC," *IEEE Transactions on Antennas and Propagation*, Vol. 56, 1763–1774, 2008.
18. Aftanas, M., *Through-wall Imaging with UWB Radar System*, Dissertation thesis, Department of Electronics and Multimedia Communications, Faculty of Electrical Engineering, Technical University of Kosice, 2009.
19. Prada, C. and J.-L. Thomas, "Experimental subwavelength localization of scatterers by decomposition of the time reversal

operator interpreted as a covariance matrix," *The Journal of the Acoustical Society of America*, Vol. 114, 235–243, 2003.

20. Minonzio, J. G., et al., "Theory of the time-reversal operator for a dielectric cylinder using separate transmit and receive arrays," *IEEE Transactions on Antennas and Propagation*, Vol. 57, 2331–2340, 2009.
21. Ahmad, F., et al., "Synthetic aperture beamformer for imaging through a dielectric wall," *IEEE Transactions on Aerospace and Electronic Systems*, Vol. 41, 271–283, 2005.
22. Solimene, R., et al., "Three-dimensional through-wall imaging under ambiguous wall parameters," *IEEE Transactions on Geoscience and Remote Sensing*, Vol. 47, 1310–1317, 2009.
23. Nikolic, M. M., et al., "Estimating distributed objects inside buildings by moving sensors," *The 23nd Annual Review of Progress in Applied Computational Electromagnetics Society (ACES)*, 409–414, Verona, Italy, 2007.
24. Genyuan, W. and M. G. Amin, "Imaging through unknown walls using different standoff distances," *IEEE Transactions on Signal Processing*, Vol. 54, 4015–4025, 2006.
25. Muqaibel, A. H. and A. Safaai-Jazi, "A new formulation for characterization of materials based on measured insertion transfer function," *IEEE Transactions on Microwave Theory and Techniques*, Vol. 51, 1946–1951, 2003.
26. Thanh, N. T., et al., "Comparison of basic inversion techniques for through-wall imaging using UWB radar," *European Radar Conference 2008, EuRAD 2008*, 140–143, 2008.
27. Chambers, D. H. and J. G. Berryman, "Target characterization using decomposition of the time-reversal operator: Electromagnetic scattering from small ellipsoids," *Inverse Problems*, Vol. 22, 2145–2163, 2006.
28. Komilikis, S., et al., "Characterization of extended objects with the D.O.R.T. method," *IEEE Ultrasonics Symposium*, Vol. 2, 1401–1404, 1996.
29. Aubry, A., et al., "Gaussian beams and Legendre polynomials as invariants of the time reversal operator for a large rigid cylinder," *The Journal of the Acoustical Society of America*, Vol. 120, 2746–2754, 2006.
30. Davy, M., J.-G. Minonzio, J. de Rosny, C. Prada, and M. Fink, "Influence of noise on subwavelength imaging of two close scatterers using time reversal method: Theory and experiments," *Progress In Electromagnetics Research*, Vol. 98, 333–358, 2009.